Design and Analysis of an Electrically Controlled Permanent Magnet Excited Synchronous Machine

Ryszard Palka, Piotr Paplicki, and Marcin Wardach

West Pomeranian University of Technology, Department of Power Systems and Electrical Drives,
Sikorskiego 37, 70-313, Szczecin, Poland

In this paper, a unique type of machine – namely, the Electrically Controlled Permanent Magnet Excited Synchronous Machine (ECPSM) possessing field weakening capability - is proposed and tested. The key is to incorporate a simple fixed DC coil into a stator of the machine. Thus, the resulting new type of motor can offer effective flux control. The design method of the ECPSM machine is presented in detail. By combining the use of GOT-It-software and the Flux3D application for the optimization of a finite element model, the static and transient electromagnetic performance are investigated. Experimental results of the ECPSM are given to verify the validity of the proposed machine.

***Index Terms*—Electric vehicles, finite element methods, optimization, permanent magnet machines.**

I. Introduction

PERMANENT magnet brushless (PMBL) machines have become more widely used for a variety of industrial applications due to their high efficiency, high power density, high drive performance and maintenance-free qualities. However, they are used in modern drives for electro-mobiles and often suffer from uncontrollable flux, thus limiting their constant power operation for EVs in high speed regions. There are many ways of solving this problem that have been described in literature [1]-[8] e.g.

The purpose of this paper is to present an advanced computation and optimization method for the 3D finite element model (FEM) of the ECPS machine that contains both PMs and the dc field control coil to increase (full) or decrease (weak) the magnetization level of the machine [9].

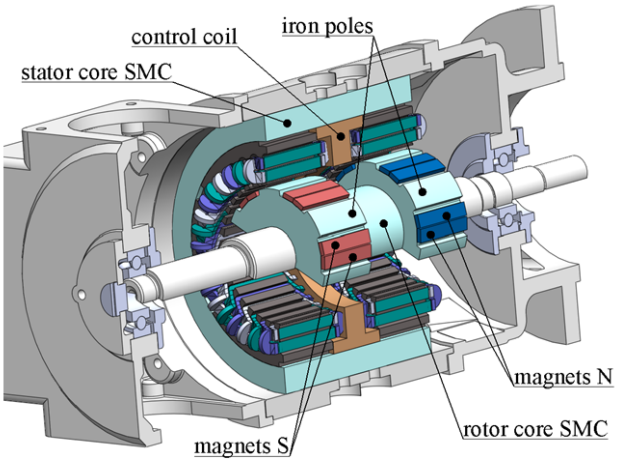

Fig. 1. Cross section of the initial ECPSM with the double surface-mounted PM rotor and three-phase windings stator structure with a fixed excitation control coil.

Manuscript received June 28, 2013. Corresponding author: R. Palka (e-mail: rpalka@zut.edu.pl).
Digital Object Identifier inserted by IEEE

II. Machine Design

Figure 1 shows a prototype ECPSM motor, which adopts a three-phase 12-pole double inner rotor topology. In the two core stators, the armature windings are located in 36 slots. The main design date of the initial ECPSM machine prototype is listed in Table I.

TABLE I
MAIN DESIGN DATA

Rated power	1.0 kW
Speed range	0-3000 rpm
Rotor outer diameter	76.5 mm
Stator outer diameter	165.0 mm
Stack length	2x40.0 mm
Air-gap length	3.0 mm
NdFeB-PM dimensions (width×thickness)	8×3 mm
NdFeB-PM remanence	1.2 T

The experimental results of both the capability of line flux control and the dynamic performance of the ECPSM partially shown in Fig. 2a, are employed to control both armature current and *dc*-field control coil current, have been done on an experimental setup shown in Fig. 2b. Initial results of these studies demonstrated insufficient voltage control range.

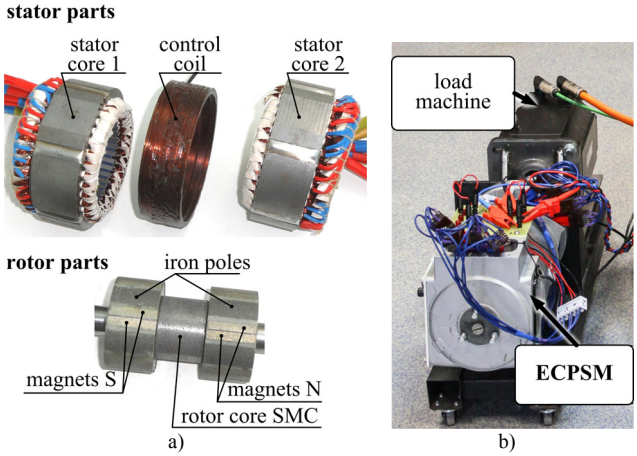

Fig. 2. ECPSM machine. (a) Stator and rotor parts. (b) Experimental setup

In order to find a better design solution for the ECPSM machine, its wide field weakening capability, high power density and high efficiency were taken into account during the finite element analysis (FEA).

III. Performance Analysis

The purpose of this study was to find the optimal thickness of magnet – d_1 and length of the two air-gaps: in front of the PM pole -$\delta_{m,}$ and in front of the iron pole -δ_{ip}, to increase range of flux control. During the finite element analysis (FEA), the geometric parameters have been varied and explored in range: d_1=1-5mm, δ_m, δ_{ip}=0.5-4.0 mm.

In order to perform the analysis of the magnetic field, a finite-element model of the device was developed taking the B-H non-linearity into account. The determination of all features of the ECPSM-machine (torque, back-EMF and field-weakening properties) is possible by using the 3D-calculation model.

A 3D FEModel 1 (initial structure) of the ECPSM machine shown in Fig. 3 has been performed according to the given criteria and fine numerical evaluation by using the optimization tool GOT-It and Flux3D ver.10.4 released by CEDRAT [10].

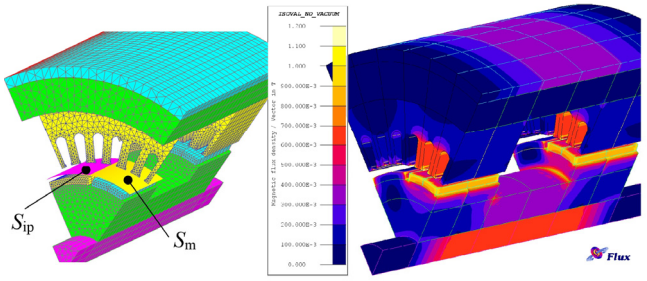

a) b)

Fig. 3. FEModel 1 of ECPSM machine. (a) Air-gap face integral. (b) Magnetic field distributions.

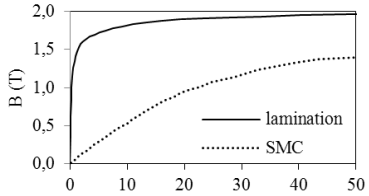

Fig. 4. Magnetization curves of a laminated material and an SMC.

Figure 4 show magnetization curves for laminated steel and for a soft material composite (SMC) which have been used in the prototype machine and during the FEA.

In order to confirm the accuracy of the FEModel 1, its FEA results were compared with some experimental results.

Figure 5a shows a no-load back-emf waveform at 1000 rpm speed and different magnetization levels (excitation current control coil I_{dc}) obtained using the FEA method and through experimentation. In addition, table II lists the root mean square (RMS) of back EMF, ΔV -back EMF full to weak magnetization level ratio, average torque T_{av}, and the dimension on geometric parameters d_1,δ_1,δ_2 for the initial FEModel 1 and the optimized FEModel 2.

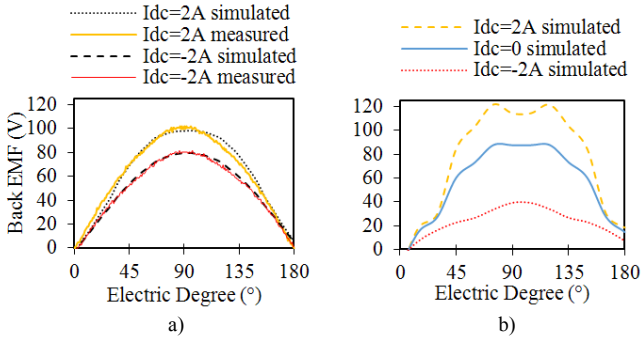

a) b)

Fig. 5. Back EMF waveforms under different magnetization level. (a) FEModel 1 and measured ECPSM machine. (b) FEModel 2.

TABLE II
BACK EMF (AT 1000 rpm), RATED TORQUE AT DIFFERENT CURRENT CONTROL COIL, GEOMETRIC PARAMETERS AND FACTORS

		Simulated			Measured		
	I_{dc} (A)	-2.0	0	2.0	-2.0	0	2.0
Model 1 initial	Back EMF(V)	63.0	56.6	71.3	62.0	56.1	71.0
	ΔV	1.13			1.14		
	T_{av} (Nm)	2.7	3.3	4.1	2.9	3.3	3.8
	$d_1/\delta_m/\delta_{ip}$ (mm)	3/3/3					
	$\Delta B_1/\Delta B_2/\Delta B_m/\Delta B_{ip}$ (T)	0.51/0.33/0.26/0.44			-		
Model 2 optimal	T_{av} (Nm)	1.9	3.51	5.8	-	-	-
	Back EMF(V)	26.5	64.9	88.6	-	-	-
	ΔV	3.34			-		
	$d_1/\delta_m/\delta_{ip}$ (mm)	3.915/3.78/1.2			-		
	$\Delta B_1/\Delta B_2/\Delta B_m/\Delta B_{ip}$ (T)	0.67/0.21/0.19/0.64					

IV. Optimization Problem

The goal of the design was to optimize the rotor iron pole and magnet shape for the length of the air-gaps in order to obtain a maximal increase in flux control range and rated torque. Hence the objective functions were specified as:

$$f_1(\mathbf{x}) = Abs(\Phi_m(\mathbf{x}) - \Phi_{ip}(\mathbf{x})) \quad (1)$$

$$f_2(\mathbf{x}) = k_1\Phi_{mi}(\mathbf{x}) - \Phi_m(\mathbf{x}) \quad (2)$$

where $k_1 = 0.8$ is the acceptable reducing magnet flux coefficient, $\mathbf{x}$ is a vector of design variables, Φ_m, Φ_{mi}, Φ_{ip}, are magnetic flux components passing through the air gap created by PM, PM at initial FEModel 1 and iron pole respectively, were calculated as:

$$\Phi_m = \iint_{S_m} \mathbf{B} \cdot d\mathbf{S} \quad (3)$$

$$\Phi_{ip} = \iint_{S_{ip}} \mathbf{B} \cdot d\mathbf{S} \quad (4)$$

By minimizing (1), the difference between the magnet and iron pole fluxes, the component becomes small and thus increased flux control range is obtained. It should be pointed out that the optimization objective and constraint functions should be calculated during the weakening magnetic field.

A 3D constrained optimization problem was implemented

based on the aggregated objectives function $f_1(\mathbf{x})$ (to be minimized) and the inequality constraint function $f_2(\mathbf{x})$ (to be ≤ 0). In order to find the global optimum for an optimization problem, a chaining optimizer has been used, containing two optimizers: a genetic algorithm (GA) and a sequential quadratic programming (SQP), as well as a seed for the pseudo-random generator. A maximum number of generations (iterations) equal to 100 and the size of the population equal to 30 have been used in the GA algorithm. In SQP, the algorithm used a maximum number of iterations, equal to 20, and a tolerance of 1.0e-6.

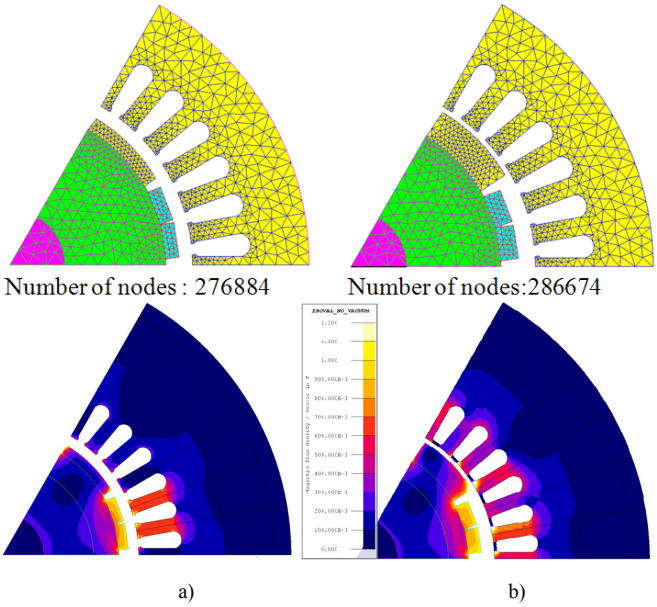

Fig. 6. Topology comparison. (a) FEModel 1. (b) FEModel 2.

Accordingly to the problem formulation, a vector of design variables **x** has been defined: $\mathbf{x}=(d_1,\delta_1,\delta_2)$. The optimization of the machine takes approximately 15 hours.

Figure 6 shows the topology comparison of the FEModel before and after performing the optimization. As can be seen, the area of the iron pole optimized model has increased substantially by reducing the air-gap length. Results show that an increase in the range of field control can be achieved by differing the length of the air-gaps. The magnet air-gap should be larger than the air-gap in front of the iron pole.

Figure 7 illustrates 3D flux density distribution over one pole section of the entire air-gap FEModel 1-2 for three different cases of the *dc* field current (-2000-,0-, and +2000-A turns) and proves, firstly the principles of the air gap magnetic flux control and secondly improving flux control weakening and strengthening. The field control capability is clearly observed in the optimized FEModel 2.

Figure 8 presents the magnetic flux distribution and the mean value of magnetic flux density over the magnet and iron pole sections of the rotor for two different cases of the *dc* field current excitation. When compared to the initial model, the optimal model (FEModel 2) displays increased sensitivity to changes in magnetization level. The air-gap magnetic flux in front of the iron pole changes its direction and magnitude in a dynamic manner (ΔB_{ip}), depending on the direction of the *dc* field current.

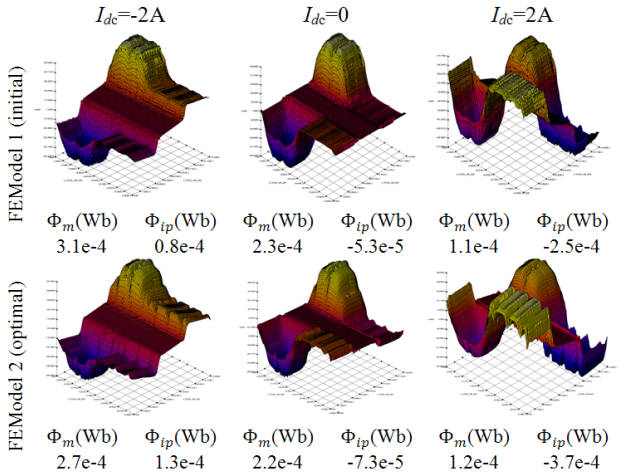

Fig. 7. 3D air-gap normal component flux density distribution and magnetic flux Φ_m, Φ_{ip} magnet and iron pole component respectively.

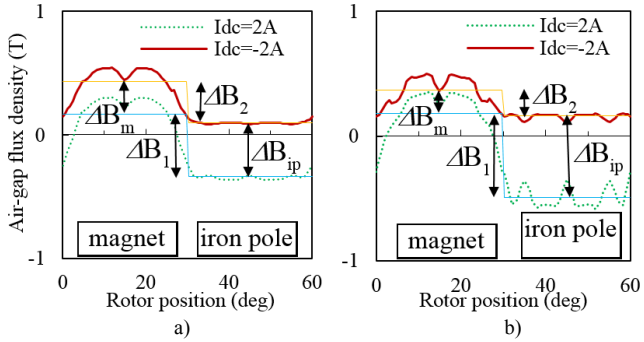

Fig. 8. Air gap flux density. (a) FEModel 1-initial. (b) FEModel 2-optimal

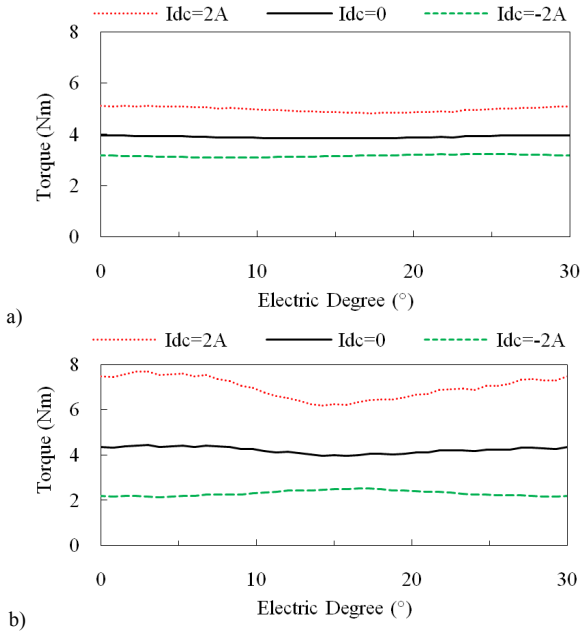

Fig. 9. Electromagnetic torque comparison by FEA. (a) FEModel 1-initial. (b) FEModel 2-optimal.

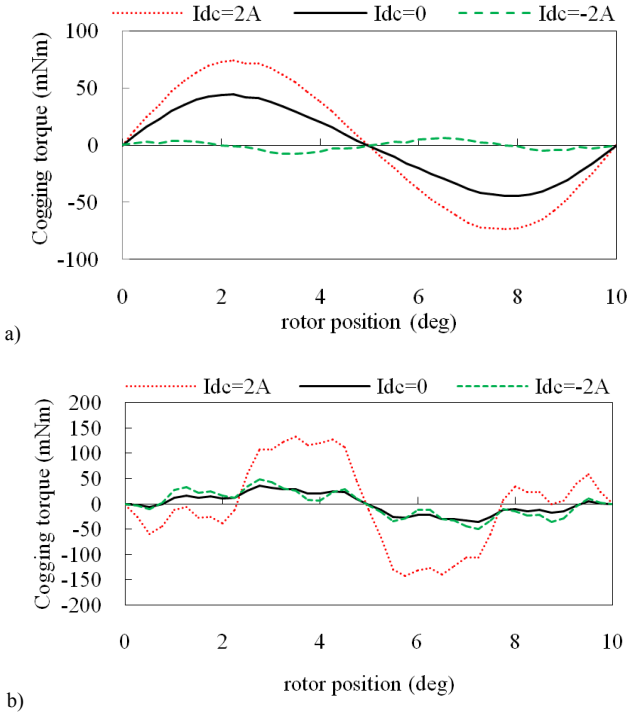

Fig.10. Cogging torque comparison by FEA. (a) FEModel 1-initial. (b) FEModel 2-optimal.

Since the PM magnetic fluxes change slightly (ΔB_m) with the field current, the total flux in the air-gap alters with the direction of the field current and the magnitude. The maximal range of flux control can be achieved if ΔB_2 tends towards zero. The maximal value of ΔB_1 means a significant strengthening of magnetic flux. In general, it can be assumed that the ratio of ΔB_1 to ΔB_2 determines a field-weakening ratio.

Electromagnetic torque characteristics of the FEModel 1 and 2 as a function of *dc* field control are shown in Fig. 9. As can be seen from these characteristics, electromagnetic torque in FEModel 2 increases about 40% at full magnetization level and decreases about 30% at weakening field compared to the FEModel 1.

Figure 10 shows the cogging torque versus rotor position. It should be noted that the disadvantage of the FEModel 2 is increasing gap harmonic and the maximum cogging torque in consequence the torque ripple at full magnetization level.

V. Conclusion

In this paper, the design and analysis of the new ECPSM machine have been presented and discussed. Thanks to the new optimization tool GOT-It, it was possible to set up an optimization problem easily and quickly, and to find the best configurations of the machine in accordance to the design objectives and the associated constraints. The relationships between the main design parameters and performance requirements have been established. By employing a simulation model in the time-stepping FEA, the online magnetization characteristic of the motor is successfully obtained. The comparison between the experimental results and the results achieved from a 3D FEModel of the machine, using an advanced coupling technology computation method, has revealed a satisfying level of accord. Moreover, the optimized results show that the proposed machine can offer effective online flux control and a wide constant-power speed range. By optimizing the shape and position of the PMs and the iron poles in the rotor, the performance of the proposed machine has been improved even further, making it more suitable for its application in EVs.

Attention should be drawn to the ratio of the EMF values that are changed from the maximum value to the minimum value. According to the optimized FEA simulation results contained in table II, it can be concluded that a field-weakening ratio of 3.3:1 and higher can be obtained. The control range, back EMF, torque output, and cogging torque component have also been analyzed. It has been demonstrated that the idea allows to easily achieving control of the radial gap machine without any negative effects of current injection.

Acknowledgment

This work has been created with the support of the Ministry of Education and Science, Poland, under grant N N510 508040.

References

[1] K. Ki-Chan, “A Novel Magnetic Flux Weakening Method of Permanent Magnet Synchronous Motor for Electric Vehicles,” *IEEE Trans. Magn.*, vol. 48, no. 11, pp. 4042-4045, Nov. 2012.

[2] X. Zhu, L. Quan, D. Chen, “Design and Analysis of a New Flux Memory Doubly Salient Motor Capable of Online Flux Control,” *IEEE Trans. Magn.*, vol. 47, no. 10, pp. 3220-3223, Oct. 2011.

[3] T. Kosaka, M. Sridharbabu, M. Yamamoto, and N. Matsui, “Design studies on hybrid excitation motor for main spindle drive in machine tools,” *IEEE Trans. Ind. Electron.*, vol. 57, no. 11, pp. 3807–3813, Nov. 2010.

[4] S. Chaithongsuk, B. Nahid-Mobarakeh, J. Caron, N. Takorabet. F. Meibody-Tabar, “Optimal Design of Permanent Magnet Motors to Improve Field-Weakening Performances in Variable Speed Drives,” *IEEE Trans. Ind. Electron.*, vol. 59, no. 6, pp. 2484-2494, June 2012.

[5] K.I. Laskaris, A.G. Kladas, “Optimal Power Utilization by Adjusting Torque Boost and Field Weakening Operation in Permanent Magnet Traction Motors,” *IEEE Trans. Energy Conversion*, vol. 27, no. 3, pp. 615-623, Sept. 2012.

[6] B. Nedjar, S. Hlioui, Y. Amara_, L. Vido, M. Gabsi, and M. Lécrivain, ”A New Parallel Double Excitation Synchronous Mac,” *IEEE Trans. Magn.*, vol. 47, no. 9, pp. 2252-22-60, Sept. 2011.

[7] M. Aydin.; H. Surong, T.A. Lipo, ”Design, Analysis, and Control of a Hybrid Field-Controlled Axial-Flux Permanent-Magnet Motor,” *IEEE Trans. Ind. Electron.*, vol. 57, no. 1, Jan. 2010, pp. 78-87.

[8] H. May, R. Palka, P. Paplicki, S. Szkolny, M. Wardach, “Comparative research of different structures of a permanent-magnet excited synchronous machine for electric vehicles,” *Electrical Review*, R. 88 NR 12a/2012, pp. 53-55.

[9] P. Di Barba, M. E. Mognaschi, R. Palka, P. Paplicki, S. Szkolny, “Design optimization of a permanent-magnet excited synchronous machine for electrical automobiles,” *International Journal of Applied Electromagnetics and Mechanics, IOS Press*, vol. 39, Number 1-4/2012, pp. 889-895.

[10] GOT-It Tutorial, Optimization software for devices and systems in electrical engineering, CEDRAT, October 2011 (http://www.cedrat.com).